International Journal of Information, Control and Computer Sciences
ISSN: 2517-9942
Vol:4, No:1, 2010

Multiscale Analysis and Change Detection Based on a Contrario Approach

F.Katlane, M.S.Naceur and M.A.Loghmari

***Abstract*—**Automatic methods of detecting changes through satellite imaging are the object of growing interest, especially beca²use of numerous applications linked to analysis of the Earth's surface or the environment (monitoring vegetation, updating maps, risk management, etc...). This work implemented spatial analysis techniques by using images with different spatial and spectral resolutions on different dates. The work was based on the principle of control charts in order to set the upper and lower limits beyond which a change would be noted. Later, the a contrario approach was used. This was done by testing different thresholds for which the difference calculated between two pixels was significant. Finally, labeled images were considered, giving a particularly low difference which meant that the number of "false changes" could be estimated according to a given limit.

***Keywords*—**multi-scale, a contrario approach, significant thresholds, change detection.

I. Introduction

CHANGE detection is a vast subject, for which many methods have been proposed, notably by Coppin [1] and Lu [2]. These methods were classified by Ola [3] according to the level of intervention and which are broken down into the following:

- *On the pixel level*: analysis by change vectors, simple detectors and regression;
- *On the characteristic level*: texture analysis, principal components analysis, analysis of shape, difference vegetation index and wavelets;
- *On the object level*: methods of direct multi-date classification, post-classification comparison and fuzzy post-classification comparison, artificial intelligence, artificial neuron networks and expert systems.

F. Katlane is with the Laboratory of Remote Sensing and Information System for spatial reference, from the National School of Engineers of Tunis, BP37, Tunis le belvédère, 1002 TUNISIE (corresponding author to provide phone: 21671874700; fax: 21671872729; e-mail: faten.katlane@ enit.rnu.tn).

M. S. Naceur is with the Laboratory of Remote Sensing and Information System for spatial reference, from the National School of Engineers of Tunis, BP37, Tunis le belvédère, 1002 TUNISIE (e-mail: MohamedSabeur.Naceur@insat.rnu.tn).

M. A.Loghmari is with the Laboratory of Remote Sensing and Information System for spatial reference, from the National School of Engineers of Tunis, BP37, Tunis le belvédère, 1002 Tunisie (e-mail: MohamedAnis.Loghmari@isi.rnu.tn).

Change detection means detecting and locating areas having evolved between two observations (or more) of the same place. These changes can be useful [4]:

- In tracking soil use, meaning the development of vegetation or the detection of seasonal changes in vegetation,
- In managing natural resources during urban development and deforestation, etc...
- In mapping out damages due to natural disasters such as volcanic eruption, tidal wave, earthquake or flood.

The *contrario* detection method is a new method in imagery. It was inspired by psychological research on vision in order to imitate the human brain. The mechanism of this detection was studied by psychologists whose conclusion indicated that the human brain locates, and then detects, events in an image [5].

The research initiated in the late 90s by Desolneux, Moisan and Morel [6] aimed at developing a quantitative theory for visual perception based on the Gestalt laws.

A contrario detection consists of determining the threshold from which the *a priori* model is no longer the one observed, but obviously an event which is detected as a difference compared to the *a priori* model [7].

Despite the relevancy of their qualitative observations on perception, the Gestaltic school could not answer the quantitative questions to determine the threshold beyond which a geometric structure is drowned in noise and therefore no longer visible by our perception [8].

Spatial resolution is the size of a pixel on the ground and comparing two images having different resolutions becomes difficult.

The method of disaggregation of information as well as fusion methods like morphological pyramid or wavelet decomposition has all been used to solve the problem of multi-scale or multi-resolution analysis on remote sensing or in subpixelic analysis [9].

Robin is the first to have considered change detection and sub-pixel classification using satellite image processing to monitor continental surfaces over time. By using an *a contrario* probability criteria which measures coherence in the sequence of "low-resolution" images and a previous reference point represented by a high-resolution classified image, Robin defined the *Number of False Alarms (NFA)* associated with a sub-field where the change pixels thus correspond with a complementary field [9].

The limits presented by these methods can be found in the difficulty of choosing an *a priori* threshold and the sensitivity to the natural variability of observations from one year to another (shifting of the seasons, ...).

The work undertaken here was divided into two parts: multi-scale analysis and change detection based on an *a contrario* approach.

The question asked was the following: how can changes be detected in high and low-resolution satellite images based on Statistical Process Control (SPC) methods?

Moreover, the reasoning proposed for change detection in the low and high-resolution satellite images based on the a *contrario* approach responded to the question: at what thresholds the calculated difference between two pixels is significant?

II. Methodology

A. Data And Processing

Multi-scale analysis is a preliminary step or pre-processing of data for change detection because it allows us to detect changes occurring in several satellite images with different resolutions.

The data used for the multi-scale analysis was characterized by:

- Their spatial resolution which is the size on the ground of the pixels,
- Their spectral resolution which is the width of the spectral bands detected,
- Their temporal resolution which is the interval between two images of the same point and depends on the satellite's orbit.

The images delivered by sensors with different characteristics distinguish geometric structures depending on spatial resolution [10].

This work played around with four images taken on different dates with different resolutions. Each image was segmented into six clusters. The images were classified according to the Expectation-maximization algorithm (EM) which is done by passing through [11]:

- An expectation step (E),
- A maximization step (M), where the maximum likelihood of the parameters is estimated by maximizing the likelihood found in step (E).
- The parameters found in (M) for a new phase of evaluating the expectation.

The method adopted for the multi-scale analysis is based on the principle of control charts. This principle consists of determining lower and upper limits. Limits were calculated beyond which a change was noted. The limits are set in such a way that if $\overline{\mu}_{C_i}$ is the average mean of a cluster c_i and $\overline{\sigma}_{c_i}$ is the average standard deviation, then:

- The upper limits are: $LS = \overline{\mu}_{C_i} + 2\overline{\sigma}_{C_i}$
- The lower limits are: $LI = \overline{\mu}_{C_i} - 2\overline{\sigma}_{C_i}$

where $\overline{\mu}_{C_i} = \frac{\sum \mu_{C_i}}{n}$, μ_{C_i} : the average of cluster c_i including m clusters and *n* images.

And $\overline{\sigma}_{C_i} = \frac{\sum \sigma_{C_i}}{n}$, σ_{C_i} : the standard deviation of cluster c_i

The following table gives a detailed description of the characteristics of the images used.

TABLE I
DATA DESCRIPTIONS

Description	SPOT1	SPOT2	SPOT4	SPOT5
Spectral bands	B1 : 0,50-0,59 µm B2 : 0,61-0,68 µm B3 : 0,78-0,89 µm	B1 : 0,50-0,59 µm B2 : 0,61-0,68 µm B3 : 0,78-0,89 µm	B1 : 0,51-0,59 µm B2 : 0,61-0,68 µm B3 : 0,79-0,89 µm B4 : 1,58-1,75 µm	0,49 - 0,69 µm
Date	1987	1998	June 2000	28 April 2003
Resolution	10 m	20m	20 m	5 m
Pixel size	128X128	128X128	128X128	637X637

The study area chosen is located north of Tunis, bordered by a marsh named Sebkhet Ariana on the east and the Lake of Tunis and Tunis-Carthage airport on the southeast, extending to the northwest to the neighborhood of Soukra. This area is characterized by the heterogeneity of the environment, especially due to the presence of the marsh, a more or less high-traffic urban area, a green belt and streets. Table 2 gives a lexicon of the clusters present in the study area.

Due to the ease of interpretation and implementation, image differencing is without doubt the most widely used detector. Univariate image differencing (UID) consists of carrying out

TABLE II
LEXICON OF SOIL USE RELATING TO THE PROPOSED CLASSIFICATION

Cluster 1	Cluster 2	Cluster 3	Cluster 4	Cluster 5	Cluster6
Wetland	*Bare soil*	*Vegetation*	*Green belt*	*Road*	*Urban area*

the differencing pixel by pixel between the original image *I1* (or its transform) and image *I2* (or its transform):

$$I_D(i, j) = I_2(i, j) - I_1(i, j) \quad (1)$$

This method results in an image called the "differencing image" (DI), revealing changes having taken place between the two observations. The pixels from the DI image with high positive or negative values are likely to characterize changes, whereas those with near-zero values correspond to unchanged pixels [12].

B. Change detection based on the a contrario approach

The data used for a *contrario* change detection were limited to one multi-spectral image SPOT4 (256X256) dating from 2000 having a 20m resolution and to one panchromatic image SPOT5 (1024X1024) dating from 2003 with a 5 meter resolution. The model of observations in the absence of change is called the a contrario model. In this model,

significant changes are defined as being events of low probability of occurrence: an event is called ε-significant if the expectation of the number of occurrences of this event is less than ε in the a contrario model [13].

The a *contrario* approach consists of rejecting the hypothesis *H0* for the difference (*diff*) if the difference is ε-significant. The *a contrario* method is, in fact, linked to the standard framework of hypothesis tests.

The difference was calculated between two pixels from two low-resolution (*LR*) images coming from the averaged high-resolution (*HR*) image and from the real *LR* image.

The panchromatic high-resolution spatial *(HR*) SPOT5 image underwent averaging by regrouping the pixels according to the relationship of the order of magnitude of the resolution of the low-resolution (*LR*) SPOT4 image and by allocation of the average value given by all of the regrouped pixels:

$$X_m = \frac{\sum x_i n_x}{N} \quad (2)$$

X_m : Average of gray levels

x_i : Gray level of the i^{th} pixel

n_x : Gray level number

N : Pixel number of the image under consideration .

Knowing that these images were taken on two different dates *t1* and *t2* .

$$diff = [\ |LR_R(i_1) - HR_S(i_1)|,..... \\ .....,|LR_R(i_n) - HR_S(i_n)|\ ] \quad (3)$$

LR_R : real low-resolution image

HR_S : simulated high-resolution image

i_n : corresponds to the pixel index under consideration.

The *NFA* for this difference is the probability of occurrence in a random uniform environment as it has one chance in two that it take place:

$$NFA\ (diff\ ) = P^k N \quad (4)$$

N : the number of elements of the difference

K: the size of the image (256x256)

P : the probability of occurrence equal to 0.5

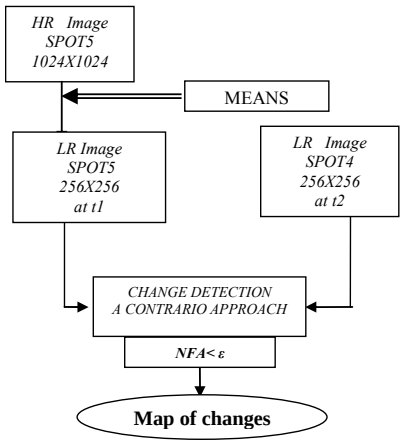

Fig. 1 Diagram of the first advance

Finally, the *NFA* was determined that was less than a *ε-significant* threshold so that:

$$NFA(|LR_R(i_1) - HR_S(i_1)|) > ... > \varepsilon > .. \\ .... > .... > .... > NFA(|LR_R(i_n) - HR_S(i_n)|) \quad (5)$$

This reasoning was tested for different thresholds:

$$\varepsilon = \{1,10^{-1},10^{-2},10^{-3},10^{-4},10^{-5},10^{-6},10^{-7},10^{-8}\}$$

At last, according to the results obtained, a map was established of the changes related to the *HR* SPOT5 and the *LR* SPOT4 images.

The same method was repeated but labeled images were taken into consideration and a ε-significant threshold was opted for. This threshold was chosen according to the control chart principle recommended in the SCP which is supposed to monitor, by statistical methods, the operational process or procedure.

Noting that if μ_{C_i} is the typical average of each cluster c_i, the difference between the estimated image *HRs*(μ_{C_i}) by (3) and observed $LR_R(i_n)$ can be measured by:

$$diff = |LR_R - HR_S| = \\ [|LR_R(\mu_{C_1} - HR_S(i_1)|.....|LR_R(\mu_{C_m}) - HR_S(i_n)|] \quad (6)$$

The related *NFA* is:

$$NFA_{(\sigma,\mu)}(diff) = [|LR_R - HR_S| \le \pm 2\sigma] \quad (7)$$

$$NFA\ (\sigma_{c_i}, \mu_{c_i})(diff\ ) = [|LR_R(\mu_{c1}) - HR_S(i_1)|..... \\ .....|LR_R(\mu_{c_m}) - HR_S(i_n)|] \le \pm 2\sigma \quad (8)$$

Success in having a particularly low difference in a LR image allowed the number of "false changes" to be estimated according to a fixed threshold equal to ± 2σ. The map of changes could thus be extracted from this procedure.

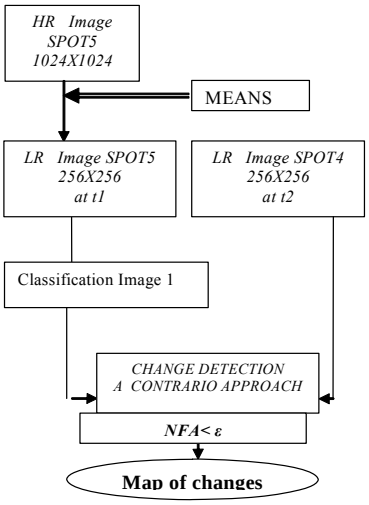

Fig. 2 Diagram of the second advance

III. Results

A. Multi-scale analysis

Spatial analysis of the images was undertaken with different spatial, spectral and temporal resolutions. It was asserted that:

I1= SPOT3 (1987), I2=SPOT3 (1998), I3= SPOT4 (2000) and *I4=SPOT5 (2003)*. Each image was segmented into 6 clusters.

The results of the multi-scale analysis are illustrated by Figures 3 through 6 which show the images classified according to the EM method.

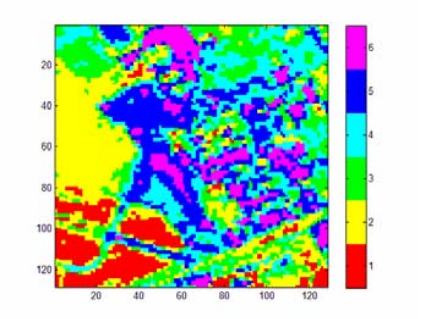

Fig. 3 Image SPOT1 classified (1987)

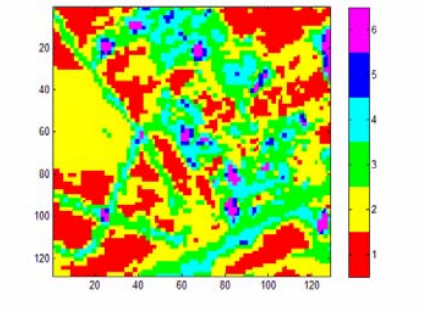

Fig. 4 Classified SPOT2 Image (1998)

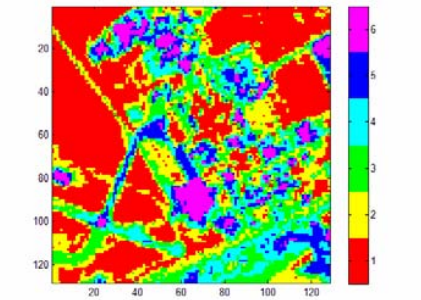

Fig. 5 Classified SPOT4 Image (2000)

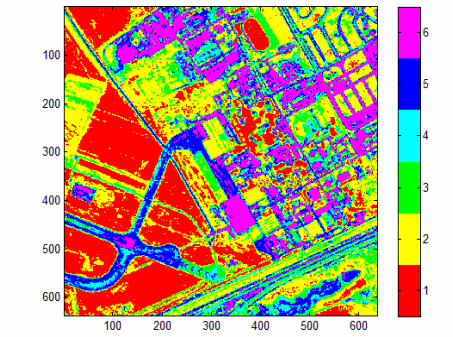

Fig. 6 Classified SPOT5 Image (2003)

Tables 3 through 6 give the average and standard deviation of each cluster.

TABLE III
AVERAGE AND STANDARD DEVIATION OF THE SPOT1 IMAGE (1987)

I1 Spot1 1987	C 1	C 2	C 3	C 4	C 5	C6
Average	28.730	75.417	112.495	144.218	177.234	212.602
Standard Deviation	17.294	12.516	17.095	17.335	15.219	18.803

TABLE IV
AVERAGE AND STANDARD DEVIATION OF THE SPOT2 IMAGE (1998)

I2 Spot2 1998	C 1	C 2	C 3	C 4	C 5	C6
Average	102.603	122.079	150.098	172.816	183.991	211.301
Standard Deviation	5.045	9.878	10.223	9.903	13.006	11.671

TABLE V
AVERAGE AND STANDARD DEVIATION OF THE SPOT4 IMAGE (2000)

I3 Spot4 2000	C 1	C 2	C 3	C 4	C 5	C6
Average	26.466	68.084	107.702	142.572	178.339	220.274
Standard Deviation	14.062	17.689	16.400	15.649	15.917	20.007

TABLE VI
AVERAGE AND STANDARD DEVIATION OF THE SPOT5 IMAGE (2003)

I4 Spot5 2003	C 1	C 2	C 3	C 4	C 5	C6
Average	13.273	51.280	101.676	146.924	182.403	224.227
Standard Deviation	7.931	20.547	19.285	18.507	16.558	16.632

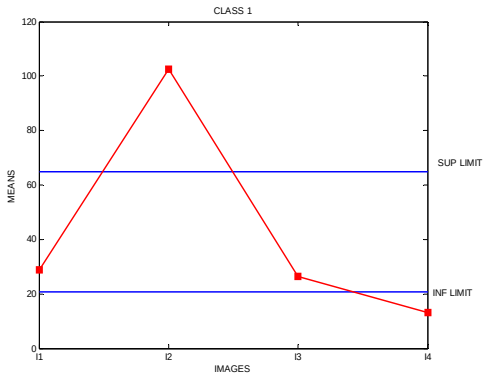

Fig. 7 Detection of changes present in several multi-resolution satellite images for cluster according to the upper and lower limit method

Figures 7 through 12 represent change detection present in images *I1, I2, I3* and *I4* for each of the clusters: { cluster 1, cluster 2, cluster 3, cluster 4, cluster 5, cluster 6} according to the upper and lower limit method. Indeed, the points outside the limits were considered to be changes.

Examination of Figure 7 compared to cluster 1 shows that there are two points which correspond to the image, *I2* and *I4,* which are outside of the limits. Cluster 1 corresponds, in fact, to wetlands and changes in this area are highly variable.

Figure 8 presents only one point outside of the limits under consideration, corresponding to image *I2* for cluster 2: bare soil.

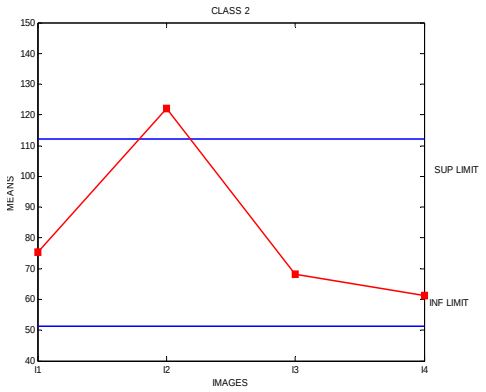

Fig. 8 Detection of changes present in several multi-resolution satellite images for cluster 2 according to the upper and lower limit method

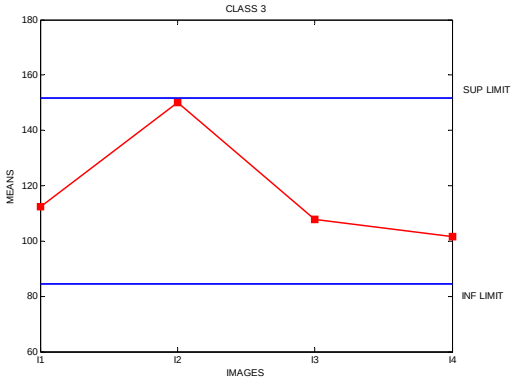

Fig. 9 Detection of changes present in several multi-resolution satellite images for cluster 3 according to the upper and lower limit method

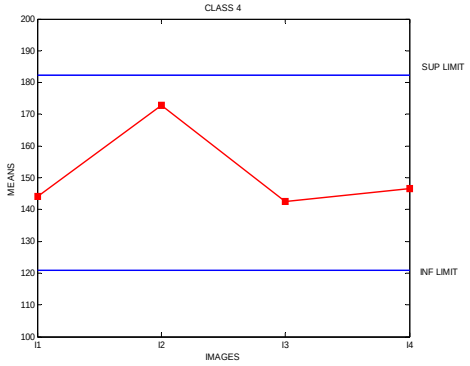

Fig. 10 Detection of changes present in several multi-resolution satellite images for cluster 4 according to the upper and lower limit method

Figures 9, 10, 11 and 12 correspond to categories 3, 4, 5 and 6 representing, respectively, vegetation, the green belt, roads and the urban area. They do not show any points outside the limits under consideration.

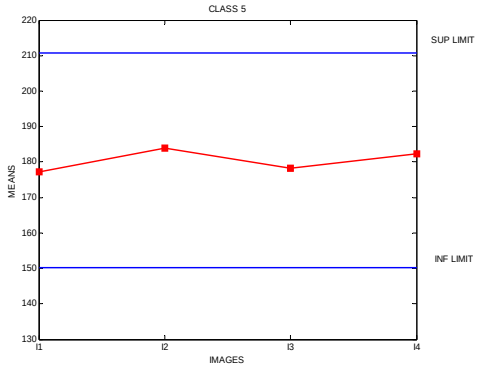

Fig. 11 Detection of changes present in several multi-resolution satellite images for cluster 5 according to the upper and lower limit method

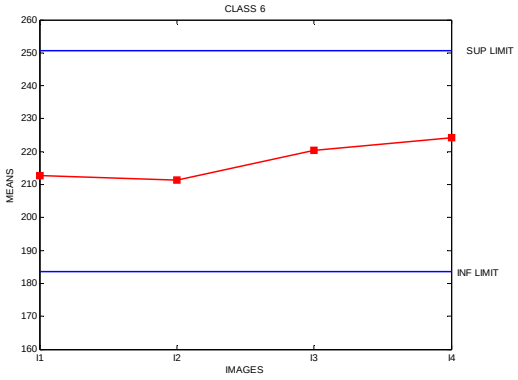

Fig. 12 Detection of changes present in several multi-resolution satellite images for cluster 6 according to the upper and lower limit method

Tables 7 through 12 give, for each image, the average of each cluster and, as well, the average mean $\overline{\mu}_{C_i}$, the average standard deviations $\overline{\sigma}_{C_i}$, the upper and lower limits beyond which there are changes and the proportion of considered cluster occupancy for each image.

TABLE VII
AVERAGE AND STANDARD DEVIATION OF CLUSTER 1

Cluster 1	I1	I2	I3	I4	Mean Of The Averages
Average	28.730	102.603	26.466	13.273	42.768
Standard Deviation	17.294	5.045	14.062	7.931	11.083
				Lower Limit	20.602
				Upper Limit	64.934

TABLE VIII
AVERAGE AND STANDARD DEVIATION OF CLUSTER 2

Cluster 2	I1	I2	I3	I4	Mean Of The Averages
Average	75.417	122.079	68.084	51.280	79.215
Standard Deviation	12.516	9.878	17.689	20.547	15.158
			Lower Limit		48.900
			Upper Limit		109.531

TABLE IX
AVERAGE AND STANDARD DEVIATION OF CLUSTER 3

Cluster 3	I1	I2	I3	I4	Mean Of The Averages
Average	112.495	150.098	107.702	101.677	117.993
Standard Deviation	17.095	10.223	16.400	19.285	15.751
				Lower Limit	86.491
				Upper Limit	149.495

TABLE X
AVERAGE AND STANDARD DEVIATION OF CLUSTER 4

Cluster 4	I1	I2	I3	I4	Mean Of The Averages
Average	144.218	172.816	142.572	146.924	151.633
Standard Deviation	17.335	9.903	15.649	18.507	15.349
				Lower Limit	120.935
				Upper Limit	182.330

TABLE XI
AVERAGE AND STANDARD DEVIATION OF CLUSTER 5

Cluster 5	I1	I2	I3	I4	Mean Of The Averages
Average	177.234	183.992	178.339	182.403	180.492
Typical Interval	15.219	13.006	15.917	16.558	15.175
				Lower Limit	150.142
				Upper Limit	210.843

TABLE XII
AVERAGE AND STANDARD DEVIATION OF CLUSTER 6

Cluster 6	I1	I2	I3	I4	Mean Of The Averages
Average	212.602	211.301	220.274	224.227	217.101
Standard Deviation	18.803	11.671	20.007	16.632	16.778
				Lower Limit	183.544
				Upper Limit	250.658

TABLE XIII
RATES LAND USES OF CLUSTERS OF THE SPOT4 (2000) AND SPOT5 (2003) IMAGES AND RATES OF CHANGE

	Wetlands	Bare Soil	Vegetation	Green Belt	Roads	Urban Area
Rates	C 1	C 2	C 3	C 4	C 5	C6
I3	38.58%	19.26%	16.18%	13.49%	8.47%	4.03%
I4	23.80%	31.32%	13.82%	11.11%	12.91%	7.04%
Rate Of Change	<-14.78%>	12.06%	<-2.36%>	<-2.38%>	4.44%	3.01%

The multi-scale analysis detected changes present in several satellite images with different resolutions by taking into consideration the upper and lower limits based on the control charts principle. Examining Table 13 shows a spatial-temporal variation of changes in the rates of land uses from 2000 to 2003, even if the multi-scale analysis carried out performed was only qualitative. The variations in clusters 1 (<-14.78%>), 3 (<-2.36%>) and 4 (<-2.38%>) are understandable. In fact, land uses of the wetlands, vegetation and green belt, which correspond to clusters 1, 3 and 4, respectively, decreased, whereas there was an increase on the bare soil, roads and the urban area which correspond respectively to clusters 2, 5 and 6.

B. Change detection based on the a contrario theory

The results of applying the first advance are shown in Figures 13 to 21. Table 16 provides the rates of change of land uses depending on the thresholds ε.

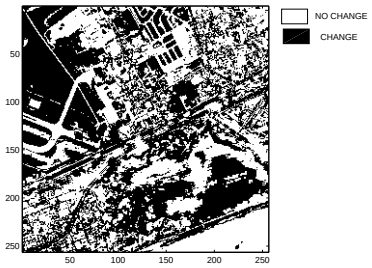

Fig. 13 Map of change for $\varepsilon=10^{-8}$

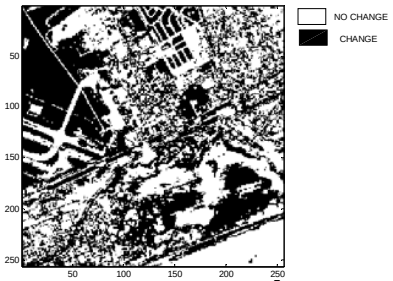

Fig. 14 Map of change for $\varepsilon=10^{-7}$

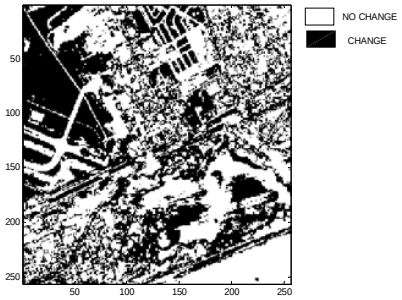

Fig. 15 Map of change for $\varepsilon=10^{-6}$

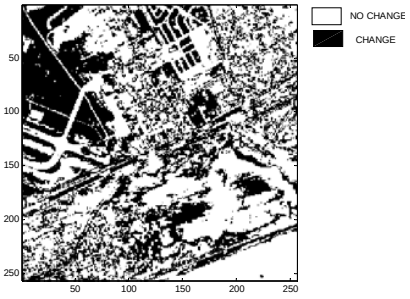

Fig. 16 Map of change for $\varepsilon=10^{-5}$

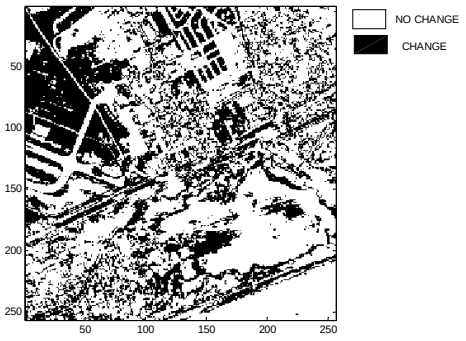

Fig. 17 Map of change for $\varepsilon=10^{-4}$

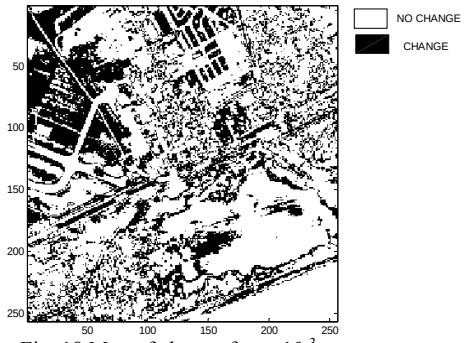

Fig. 18 Map of change for $\varepsilon=10^{-3}$

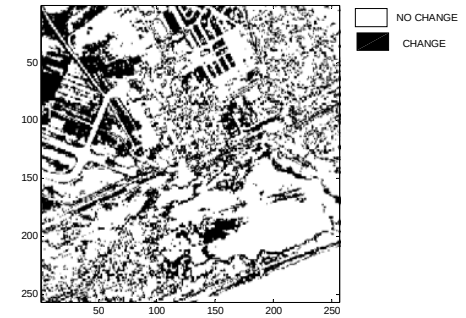

Fig. 19 Map of change for $\varepsilon=10^{-2}$

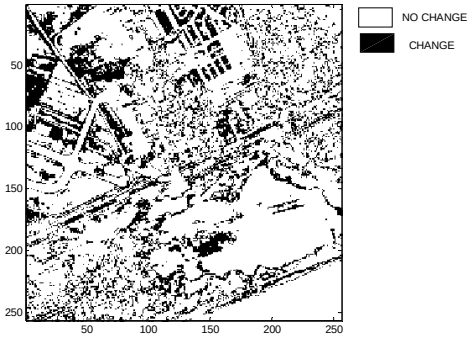

Fig. 20 Map of change for $\varepsilon=10^{-1}$

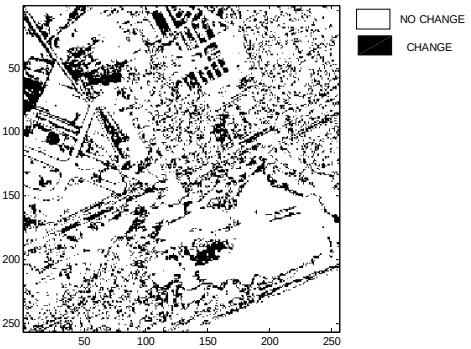

Fig. 21 Map of change for $\varepsilon=1$

The rates of change varied from *46.81%* for $\varepsilon=10^{-8}$ to *80.19%* for $\varepsilon=1$. The difference between these rates of change of the two extreme values of ε, is high (*33.38%*). It was noted that the lower ε is, the lower the rate of change is as well. These results were compared to real rates of land uses obtained by applying a standard method of change detection based on differencing (ID).

The results of applying the second advance are depicted in Figure 22. Table 15 gives the rates of change, false change or false alarm and no change.

Fig. 22 Map of change relative to the second advance

TABLE XV
PROPORTION OF CHANGE / NO CHANGE / FALSE CHANGE WHEN APPLYING THE SECOND ADVANCE

Method	Change	No change	False change (false alarm)
a *contrario* threshold $\varepsilon=\pm 2\sigma$	47.06%	13.45%	39.49%

The results of Table 16 show that applying the standard method of change detection based on differencing gives, on one hand, a rate of change close to that of the first advance when the threshold ε=1. On the other hand, it gives a rate of no change closer to the rate obtained by applying the second advance.

The *a contrario* approach for change detection on high- and low-resolution satellite images allowed several thresholds to be tested according to two methods having a significant difference.

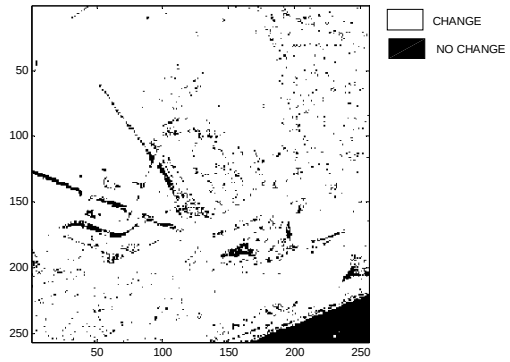

Fig. 23 Map of change relative to the (ID) method

TABLE XVI
PROPORTION OF CHANGE / NO CHANGE / FALSE CHANGE WHEN APPLYING A SIMPLE DIFFERENCING, THE FIRST METHOD AND THE SECOND METHOD

Method	Change	No change	False change (false alarm)
Standard differencing (DI)	86.83%	13.17%	
a contrario threshold ε-significant	46.81%	53.19%	
$\varepsilon=10^{-8}$	49.69%	50.31%	
$\varepsilon=10^{-7}$	53.14%	46.86%	
$\varepsilon=10^{-6}$	58.34%	41.66%	
$\varepsilon=10^{-5}$	62.07%	37.93%	
$\varepsilon=10^{-4}$	66.07%	33.93%	
$\varepsilon=10^{-3}$	70.22%	29.78%	
$\varepsilon=10^{-2}$	76.01%	23.99%	
$\varepsilon=10^{-1}$	80.19%	19.81%	
$\varepsilon=1$			
a *contrario* threshold $\varepsilon=\pm 2\sigma$	47.06%	13.45%	39.49%

IV. DISCUSSIONS AND CONCLUSION

The method of multi-scale analysis developed here has enabled the detection of change whatever the image resolution and number of images tested. Indeed, the points outside the limits calculated for each class will be regarded as changes.

The multi-scale analysis, in case of occurrence of sudden changes, activates an alarm in the event of the advent of any natural phenomenon or the occurrence of a disaster (fires, avalanches, floods ...).In this case, it was shown that there were two points in images *I2* and *I4* which were outside of the set limits. It was known that these changes correspond to the wetlands and that changes in this area are highly variable.

In addition, changes to the bare soil were able to be located on image *I2*. As for the other clusters representing vegetation, the green belt, roads and the urban area, no points were found outside of the limits taken into consideration. However, this result does not mean that there no changes occurred in these areas, but indicates that the calculated limits need to be reconsidered.

The advantage of this method is that it can be done with a large number of images with different resolutions, whatever the magnitude of the images.

The disadvantage of this method, however, is that, first of all, it is not quantifiable. Secondly, it is applied cluster by cluster, thereby necessitating classification of the images beforehand, in order to be able to calculate averages, standard deviations and proportion of cluster occupancy.

This work could be improved by exploiting the occupancy rate of the change of clusters and trying to integrate them in the process of detecting multi-scale change.

Global rates of change would be able to be quantified and maps of change could be generated by using the *a contrario* approach to detect changes.

In addition, it should be noted that the framework proposed clearly improved results compared to the standard approach based on differencing (ID) due to the fact that the method used brought to light the proportion of false alarms.

Indeed, the results of applying the first advance provided rates of change of land uses according to a group of ε-threshold values. Only the exact value of the threshold closest to the reality remains to be defined.

The results of applying the second advance gave rates of change, false changes or false alarms and no change.

Global rates of change could be calculated using change detection based on the *a contrario* approach. A more detailed study would provide rates of change for each theme. Integration of additional information in the established change detection process would improve the approach

The results of *a contrario* change detection proposed by Robin [5] were limited by the fact that objects were only detected if their sub-pixel size was greater than 25% of the *LR* pixel. In addition, the study proposed by Robin should be compared to real situations on entire image sequences.

REFERENCES

[1] P. R. Coppin, I. Jonckheere and K. Nachaerts, " Digital change detection in ecosystem monitoring'', *Int. J. of Remote Sensing*, vol. 24, 2003, pp. 1–33 .

[2] D. Lu, P. Mausel, E. Brondizio and E. Moran, "Change detection techniques'', *Int. J. of Remote Sensing*, vol. 25, no. 12, pp. 2365–2407 (2004).

[3] H. Ola , G. J. Hay, '' A Multiscale Object-Specific Approch to Digital Change Detection,'' *International Journal of Applied Earth Observation and Geoinformation*, Volume 4, Issue 4, November 2003, Pages 311-327.

[4] C. Carincotte, "Segmentation markovienne floue d'images application en détection de changements entre images radar'', thèse à l'université Paul Cezanne Aix-Marseille, 2005.

[5] A. Desolneux, " Evénements significatifs et applications a l'analyse d'images'', PhD thesis, Ecole Normale Supérieure de Cachan, Décembre 2000.

[6] A. Desolneux, L. Moisan, and J.M. Morel, "Edge detection by Helmholtz principle'', *Journal of Mathematical Imaging and Vision*, 14(3):271 n° 284, 2001.

[7] A. Desolneux, L. Moisan and J.-M. Morel, Gestalt Theory and Computer Vision, chapter (pp.71-101) in the book Seeing, Thinking and Knowing, edited by A. Carsetti, Kluwer Academic Publishers, 2004.

[8] A. andres, "Sur quelques problèmes mathématiques en analyse d'images et vision stéréoscopique'', habilitation a dirigé des recherches

Université Paris V Rene Descartes U.F.R. mathematiques et informatique, 1 décembre 2005.
[9] R. Amandine, "Approche a contrario pour la détection de changements à partir d'images satellite basse résolution'', *GRETSI 2005* , Louvain-la-Neuve, 6-9 Septembre 2005.
[10] C. Thomas, " fusion d'images de résolutions spatiales différentes " l'Ecole des Mines de Paris, 196pages, déc 2006.
[11] G. Celeux, G,Govaert, "A Classification EM Algorithm for Clustering and Two Stochastic Versions," *Computational Statistics and Data Analysis,* vol. 14, pp. 315-332, 1992.
[12] S. Hese and C. Schmullius, "Forest cover change detection in Siberia", in *Proc. of the High Resolution Mapping from Space* Workshop, 2003.
[13] A. Desolneux, L. Moisan, and J.M. Morel. "A grouping principle and four applications", *IEEE Transactions on Pattern Analysis and Machine Intelligence*, 25(4), 508–513, April 2003.
[14] R. Amandine, " détection de changements et classification sous-pixeliques en imagerie satellitaire'', thèse université PARIS DESCARTES, 249 pages, 2007.